Mechanism of the Band Gap Opening across the Order-Disorder Transition of Si(111)(4 × 1)-In

C. González,[1,2] Jiandong Guo,[3,4] J. Ortega,[1] F. Flores,[1] and H. H. Weitering[3,5]

[1]*Departamento de Física Teórica de la Materia Condensada, Universidad Autónoma, 28049 Madrid, Spain*
[2]*Institute of Physics, Academy of Sciences of the Czech Republic, Cukrovarnická 10, 162 53, Prague, Czech Republic*
[3]*Department of Physics and Astronomy, The University of Tennessee, Knoxville, Tennessee 37996, USA*
[4]*Beijing National Laboratory for Condensed Matter Physics and Institute of Physics, Chinese Academy of Sciences, Beijing 100190, P. R. China*
[5]*Materials Science and Technology Division, Oak Ridge National Laboratory, Oak Ridge, Tennessee 37831, USA*

(Received 11 September 2008; published 17 March 2009)

The ground state properties of indium atom chains on the Si(111)8 × 2-In surface and the nature of their insulator-metal (IM) transition near 120 K are under intense dispute. We compare experimental scanning tunneling microscopy (STM) images of the low temperature (LT) 8 × 2 phase with STM image calculations from Density Functional Theory (DFT). Our LT studies clearly indicate the existence of a frozen shear distortion between neighboring atom chains, resulting in the formation of indium hexagons. Tunneling spectra furthermore indicate that the IM transition coincides with the collapse of a ~0.3 eV surface-state band gap at the Γ point of the 4 × 2 Brillouin zone. This implies that the IM transition is driven by a shear phonon, not by Fermi surface nesting.

DOI: 10.1103/PhysRevLett.102.115501 PACS numbers: 81.16.Dn, 68.35.Md, 68.37.Ef

Quasi-one-dimensional electron (1D) systems are interesting objects for exploring collective phenomena and nanoscale applications. In 1955, Peierls considered an isolated chain of metal atoms with a half-filled metallic band and made the argument that such a chain should be unstable with respect to a symmetry-lowering modulation of the atomic coordinates and valence-charge density [1]. The underlying mechanism involves the strong coupling in 1D between lattice vibrations and electrons near the Fermi level (E_F). The ground state is insulating. Inclusion of electron correlations may lead to competing ground states, such as a spin density wave, a Luttinger liquid, or even a superconductor [1].

The experimental reality can be far more complicated. A strong case in point is the Si(111)4 × 1-In system [2–17], where indium adatoms self assemble on a Si(111) surface into a double zigzag chain pattern as shown in Figs. 1(a) and 1(b). The atom chains undergo a phase transition at about 120 K, presumably of the Peierls-type, but this transition involves not just one but several surface-state bands [Fig. 1(c)] [3,7,8]. Below 120 K, the translational symmetry changes initially from 4 × 1 to 4 × 2 and then to 8 × 2, indicating a period doubling both parallel and perpendicular to the atom chains [Fig. 1(b)]. The precise structure of the LT phase and mechanism of the IM transition are controversial [3–15]. Some angle-resolved photoemission (ARPES) experiments indicate the opening of a small (~40 meV) Peierls gap below 120 K [3,7,8], but other studies indicated only a reduction in the density of states (DOS) at E_F [4–6].

On the theory side, most DFT calculations indicate pair formation of the outermost In atoms of the double zigzag chains (Fig. 1), resulting in the formation of In trimers [12–15]. However, this Peierls-like mechanism still leaves one band that crosses E_F, a puzzling result in light of the most recent ARPES measurements [7,8,16]. Very recently, some of us proposed that the Peierls-type dimerization of the outermost In atoms is accompanied by a shear distortion, whereby neighboring zigzag chains are displaced in opposite directions [13]. This mechanism leads to the formation of In hexagons rather than trimers, produces a 4 × 2 periodicity, and fully opens up a gap [Fig. 1(d)]. The 8 × 2 structure was subsequently obtained by alternating the hexagon orientation [Fig. 1(b)], producing a total energy gain of 40 meV/4 × 2-unit cell. The IM transition was attributed to dynamical fluctuations between degenerate 4 × 2 structures, producing an average 4 × 1 structure on the time scale of STM. However, the hexagon formation and dynamical fluctuation picture have yet to be confirmed experimentally.

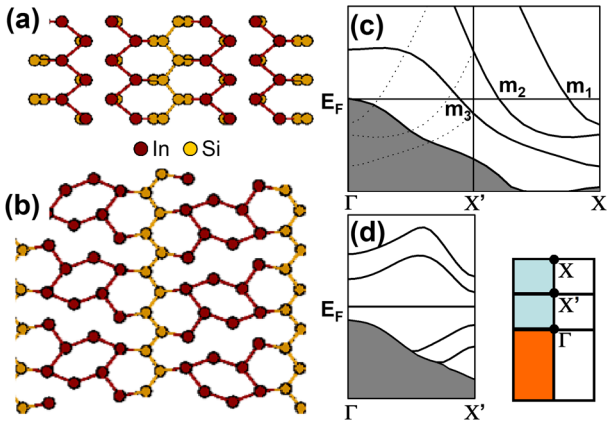

FIG. 1 (color online). Top view of the Si(111)4 × 1-In (a) and Si(111)8 × 2-In (b) surface (hexagon model; Ref. [13]). Panels (c) and (d) show the calculated 4 × 1 and 4 × 2 surface-state bands along the In chains. Brillouin zones are indicated.

In this Letter, we show that our experimental STM images of the LT 8×2 phase are in excellent agreement with STM image calculations for the hexagon structure [13,14]. We furthermore monitor the evolution of the empty states with STS and establish that the IM transition is driven by thermal excitation of a soft shear-phonon mode involving *neighboring* atoms chains. This picture is fundamentally different from a Peierls distortion *within* the In atom chains, which invokes Fermi surface nesting as the driving mechanism [3].

Experiments were carried out using a variable temperature STM. The Si(111)4×1-In reconstruction was prepared following the procedures in Ref. [11]. DFT calculations were performed following Ref. [13]. STM images and STS spectra were obtained using the nonequilibrium Green-Keldysh formalism [18,19].

Figure 2 shows registry-aligned filled- and empty-state STM images of the 8×2 phase at 42 K for different voltages, along with the simulated images from DFT. The filled-state images are almost independent of bias between 0.5 and 1.5 V. The empty-state images, on the other hand, are more strongly bias dependent. The relative brightness of the protrusions and the orientation of the block units are well reproduced by the calculations, although the 0.5 eV empty state image does reveal a minor discrepancy in the actual shape of the blobs. Interestingly, dark trenches coincide with the location of the Si rows, except for the 1.5 V empty state image where they dissect the In hexagons. The registry shift of the trenches is clearly evident in the experimental images. We also simulated the images for the trimer structure (not shown), but the agreement with experiment is poor. Note that previous image simulations for the trimer structure required artificial adjustment of E_F in order to obtain reasonable agreement with experiment because this structure is metallic in DFT [12].

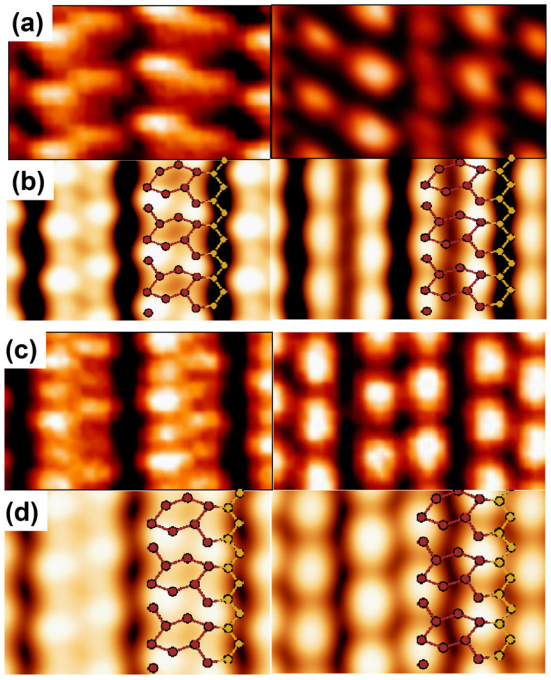

FIG. 2 (color online). Experimental (a), (c) and theoretical (b), (d) STM images with filled states on the left and empty states on the right. The tunneling bias in panels (a) and (b) is 0.5 V. The bias in panels (c) and (d) is 1.5 V.

Previous STM studies had focused on the conversion of 4×2 or 8×2 domains into the 4×1 surface, a process that begins around 90 K and completes at about 130 K [9,11]. This temperature region is characterized by strong phase fluctuations of the order parameter [9,11]. Here, we focus on the temperature dependence of the energy gap of the 4×2 domains, which is related to the amplitude of the order parameter (we find that the I-V spectra of the 4×2 and 8×2 structures are identical). STS data were acquired as a function of temperature for the following STS set-points: 0.5 V/0.5 nA, 0.5 V/1.0 nA, 0.5 V/1.9 nA, and 0.3 V/0.1 nA, which correspond to different tip-sample distances.

Figures 3(a) and 3(b) show STS data from the $4(8) \times 2$ domains plotted on linear and semilogarithmic scales, respectively, using the set point of 0.5 V/0.5 nA. We also included the spectrum of the metallic 4×1 phase at 120 K to contrast the electronic properties of the two phases. Spectra below 110 K appear very similar, showing an *almost* flat tunneling plateau between -0.1 and $+0.2$ eV.

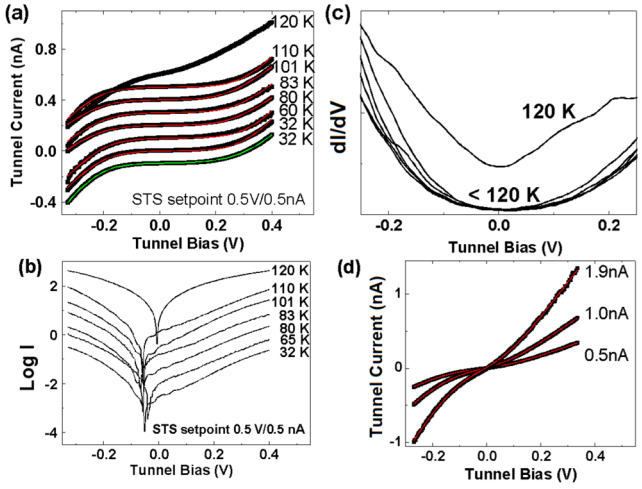

FIG. 3 (color online). (a) Tunneling spectra of the 4×2 surface at different temperatures. The solid (green) line through the bottom spectrum is a six parameter fit using Eq. (3). All other fits, represented by the solid (red) lines, employed three adjustable parameters. (b) Tunneling spectra on a semilog scale, showing a thermovoltage and thermionic I-V characteristics. (c) dI/dV spectra at various temperatures. Note the conductance offset at 120 K, signifying an abrupt IM transition. (d) Fitting of the 120 K spectra for the various STS set-points. The solid (red) lines represent the fits, assuming half-Gaussian distributions for Δ_1 and Δ_2. (All the fittings are superimposed over the experimental data curves.)

The semilog plots reveal the origin of the small STM current in this gap region. First, there appears to be a finite current at zero bias (or bias offset), which is attributed to a thermovoltage across the tunnel junction in the VT-STM setup [20]. This ≈50 meV thermovoltage quenches in the metal phase. Second, $\ln I$ versus V is strikingly linear between 0 and +0.3 V, indicating that the current is limited by thermionic emission from the metal tip. We will now derive an expression for the combined thermionic emission or tunnel current and determine the gap via a nonlinear least squares fitting procedure.

We assume that In layer has an energy gap Δ, and that E_F of the tip is located at an energy Δ_1 (Δ_2) from the conduction (valence) band edge, so that $\Delta = \Delta_1 - \Delta_2$ (with $\Delta_2 < 0$). The electron current is given by

$$I_e = A_e \int_{\Delta_1}^{\infty} dE\{n_t(E) - n_s(E)\} \quad (1)$$

where n_t and n_s are the Fermi functions for the tip and sample, respectively, and A_e is a factor that embodies: (a) a tunneling probability that depends on V as $\exp(aV)$ (a = constant), because V is much smaller than the tunneling barrier (see Eqs. 82 and 83 in Ref. [19]); and (b) the tip and sample DOS, which are assumed to be constant because only the semiconducting states within k_BT from the gap edges are relevant for the current (however, the full tip and sample DOS is used to calculate STM images for higher voltages). A similar expression applies to the hole current I_h. Integration of Eq. (1) yields

$$I_{e(h)} = A_{e(h)}\{k_BT_t \ln[1 + \exp-(+)(\Delta_{1(2)} - V)/k_BT_t] - k_BT_s \ln[1 + \exp(-(+)\Delta_{1(2)}/k_BT_s)]\} \quad (2)$$

where the T_t and T_s are the tip and sample temperatures. The total current is given by

$$I_{\text{total}} = I_e - I_h. \quad (3)$$

Equation (3) defines the current in the semiconducting phase below 120 K. Ideality factors of the electron and hole currents were included in our fitting procedure (i.e., $k_BT \rightarrow nk_BT$). They turned out to be close to $n = 2$, which is characteristic of generation or recombination processes in the space charge layer [21]. The bottom spectrum in Fig. 3(a) shows a nonlinear least squares fit using Eq. (3). By relaxing all six parameters, we obtain perfect fits for all spectra up to 110 K. The fits indicate that Δ_1 and Δ_2 are temperature independent up to the phase transition with values hovering around +0.3 and −0.2 eV, respectively. Δ_2 is attributed to the gap between E_F and the valence band maximum of bulk Si (at Γ), in good agreement with the 0.22 eV value measured by core level spectroscopy [22]. This indicates that with the chosen set points, STS only senses electronic states near Γ [23]. For instance, we do not observe any tunneling into the top of the m_2 surface-state band [3,7,8], which is located only 40 meV below E_F at the zone boundary. Δ_1 is therefore attributed to the tunnel gap between E_F and the surface states at Γ.

To analyze the I-V spectra at different temperatures and set-points, it is desirable to limit the number of free parameters. We therefore fix $n = 2$ and require that $A_e = A_h$. The remaining free parameters are Δ_1, Δ_2, and $A_{e(h)}$. The fits are still remarkably good [Fig. 3(a)] and consistently produce similar gap values: $\Delta_1 = 0.3 \pm 0.05$ eV and $\Delta_2 = -0.2 \pm 0.05$ eV for $T < 120$ K. These numbers are robust for all the different STS set points, except for the 0.5 V/1.9 nA data set. The gap values of the latter reduced to 0.25 and −0.11 eV, respectively, consistent with the fact that at short tip distances, STS becomes increasingly sensitive to states with nonzero parallel momentum [23].

Attempts to fit the 120 K spectrum with the zero-gap limit of Eq. (3) were unsatisfactory. Inspired by the possibility that the 4×1 phase is not a static structure but exhibits metal-semiconductor fluctuations [13], we fitted the I-V data assuming half-Gaussian distributions for both Δ_1 and Δ_2, centered at zero bias. The adjustable parameters are the standard deviations σ_1 and σ_2, respectively, the prefactor, and statistical bin size. These four-parameter fits produced consistent values for the standard deviations $\sigma_1 = 0.15$ eV and $\sigma_2 = 0.2$ eV for the three different STS set-points in Fig. 3d [24].

Similar gap distributions are also indicated by our first principles molecular dynamics simulations [13], where we took snapshots of the electronic band structure every 500 fs. Figures 4(a) and 4(b) show the total-gap distribu-

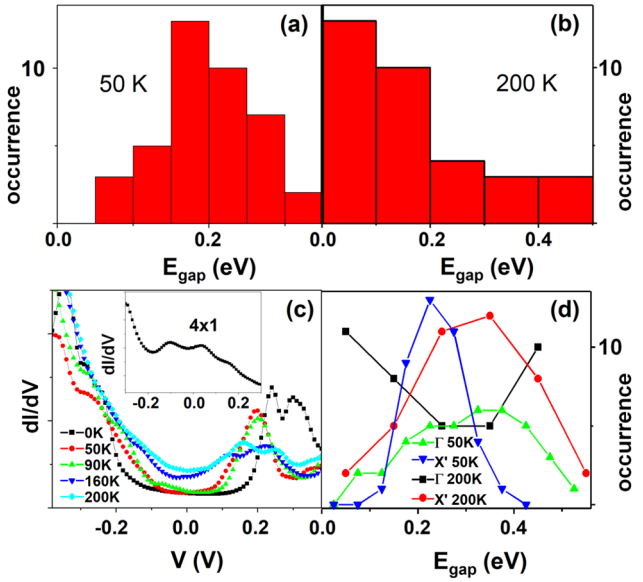

FIG. 4 (color online). Theoretical gap distributions at (a) 50 K and (b) 200 K; (c) Simulated dI/dV spectra of the 4×2 surface, showing nearly identical tunneling gaps at 50 and at 90 K and a clear conductance offset 160 and at 200 K. Inset: calculated dI/dV spectrum of a static 4×1 structure. (d) Gap distributions at the Γ and X' points at 50 and at 200 K, respectively.

tion of these snapshots at 50 and at 200 K. The gap distribution at 50 K is roughly Gaussian and is centered at about 0.18 eV, indicating that the time averaged electronic structure is nonmetallic. The 200 K case produces a (half) Gaussian centered at E_F, indicating that the time averaged electronic structure is metallic.

Theoretical dI/dV curves [18] (calculated also using a time average of the electronic band structure and neglecting the thermionic current) at 50 and at 90 K, shown in Fig. 4(c), are very similar, consistent with the experimental observation that dI/dV hardly changes between 40 and 120 K. The theoretical dI/dV spectra at 160 and 200 K are metallic, however, showing a clear conductance offset at zero bias. Notice that the spectrum of a static 4×1 structure looks completely different [Fig. 4(c): inset] and is inconsistent with experiment.

Experimentally, the IM transition is marked by the collapse of Δ_1 near the Γ-point. Theoretical snapshots of the electronic structure at the Γ and X' points of the 4×2 structure not only confirm this notion [Fig. 4(d)], but also reveal that the band gap at the zone boundary X' is much less affected by temperature. The collapse of Δ_1 implies that the HT phase should exhibit an electron pocket at the Γ-point. ARPES data indeed revealed an electron pocket, but it is located at the zone boundary or X-point of the HT 4×1 structure [3,7,8]. This pocket was denoted as the m_1 band [Fig. 1(c)] and vanishes abruptly below 120 K. Note however that in the dynamical fluctuation scenario, this X-point is symmetry equivalent with the Γ-point of the fluctuating 4×2 structure, meaning that ARPES and STS are fully consistent within the dynamical fluctuation picture. The surface-state bands of the metal phase in ARPES should thus be interpreted as superpositions of the many bands associated with the fluctuating structures [13].

The 40 meV gap at X', observed by ARPES, is much smaller than Δ_1 or Δ_2 [7,8]. While the 40 meV gap *below* E_F seems to disappear above 120 K, the Peierls gap at X' persists *above* E_F [Fig. 4(d)]. Specifically, at 200 K, it exhibits a broad distribution centered at approximately 0.3 eV above E_F. From the BCS gap equation [25], one estimates a Peierls transition temperature of the order of 1000 K. The downward shift of the m_1 electron pocket thus appears to be far more relevant for the IM transition at 120 K than the Peierls mechanism. This shift of m_1 is associated with the excitation of a shear phonon [13].

In summary, we found that the hexagon model is the most probable structure of the LT 8×2 phase, and that it is nonmetallic. The IM transition is clearly associated with the collapse of Δ_1 at Γ, which can be fully reconciled with ARPES [3,7,8], provided that the fundamental translation symmetries of the LT and HT phases are identical, namely 4×2. This supports the dynamical fluctuation scenario and rules out Fermi surface nesting as the driving mechanism of the IM transition. This atomistic interpretation of the IM transition may apply to other strongly coupled charge density wave systems where IM transitions are of the order-disorder type and unrelated to Fermi surface nesting.

We thank E. W. Plummer and P. C. Snijders for stimulating discussions. The experimental work was funded by NSF Grant No. DMR 0606485 and by Oak Ridge National Laboratory, which is supported by the Office of Science of the US Department of Energy under Contract No. DE-AC05-00OR22725. The theory component was funded by the Spanish Ministerio de Ciencia e Innovación under Grants Nos. 2007-0034 and MAT-2007-60966.

[1] G. Grüner, *Density Waves in Solids 1* (Addison-Wesley, Reading, MA, 1994).
[2] J. Nogami *et al.*, Phys. Rev. B **36**, 6221 (1987); J. Kraft *et al.*, Phys. Rev. B **55**, 5384 (1997); T. Abukawa *et al.*, Surf. Sci. **325**, 33 (1995); I. G. Hill and A. B. McLean, Phys. Rev. B **56**, 15725 (1997).
[3] H. W. Yeom *et al.*, Phys. Rev. Lett. **82**, 4898 (1999).
[4] K. Sakamoto *et al.*, Phys. Rev. B **62**, 9923 (2000).
[5] O. Gallus *et al.*, Eur. Phys. J. B **20**, 313 (2001).
[6] H. W. Yeom *et al.*, Phys. Rev. B **65**, 241307(R) (2002).
[7] J. R. Ahn *et al.*, Phys. Rev. Lett. **93**, 106401 (2004).
[8] J. R. Ahn *et al.*, Phys. Rev. B **75**, 033313 (2007).
[9] S. J. Park *et al.*, Phys. Rev. Lett. **93**, 106402 (2004).
[10] T. Tanikawa *et al.*, Phys. Rev. Lett. **93**, 016801 (2004).
[11] G. Lee, J. Guo, and E. W. Plummer, Phys. Rev. Lett. **95**, 116103 (2005).
[12] J. H. Cho, J.-Y. Lee, and L. Kleinman, Phys. Rev. B **71**, 081310(R) (2005).
[13] C. Gonzalez, F. Flores, and J. Ortega, Phys. Rev. Lett. **96**, 136101 (2006); New J. Phys. **7**, 100 (2005).
[14] A. A. Stekolnikov *et al.*, Phys. Rev. Lett. **98**, 026105 (2007).
[15] J. H. Cho and J.-Y. Lee, Phys. Rev. B **76**, 033405 (2007).
[16] Y. J. Sun *et al.*, Phys. Rev. B **77**, 125115 (2008).
[17] S. Riikonen, A. Ayuela, and D. Sanchez-Portal, Surf. Sci. **600**, 3821 (2006).
[18] P. C. Snijders *et al.*, Phys. Rev. B **72**, 125343 (2005).
[19] J. M. Blanco, F. Flores, and R. Pérez, Prog. Surf. Sci. **81**, 403 (2006).
[20] D. Hoffmann *et al.*, J. Electron Spectrosc. Relat. Phenom. **109**, 117 (2000).
[21] S. M. Sze, *Physics of Semiconductor Devices* (John Wiley and Sons, New York, 1981) 2nd ed.
[22] T. Tanikawa, Ph.D. thesis, University of Tokyo, 2003.
[23] R. M. Feenstra, J. A. Strocio, and A. P. Fein, Surf. Sci. **181**, 295 (1987).
[24] It could be argued that the LT data should also be fitted with Gaussian distributions. However, such fits would not be unique since it is possible to fit the data equally well with only three free parameters.
[25] T. Aruga, Surf. Sci. Rep. **61**, 283 (2006).